Plasma sheath structures around a radio frequency antenna

Jiannan Tu,[1] Paul Song,[1,2] and Bodo W. Reinisch[1,2]

Received 14 February 2008; revised 4 April 2008; accepted 18 April 2008; published 31 July 2008.

[1] A one-dimensional particle-in-cell (PIC) simulation code is developed to investigate plasma sheath structures around a high-voltage transmitting antenna in the inner magnetosphere. We consider an electrically short dipole antenna assumed to be bare and perfectly conducting. The oscillation frequency of the antenna current is chosen to be well below the electron plasma frequency but higher than the ion plasma frequency. The magnetic field effects are neglected in the present simulations. Simulations are conducted for the cases without and with ion dynamics. In both cases, there is an initial period, about one-fourth of an oscillation cycle, of antenna charging because of attraction of electrons to the antenna and the formation of an ion plasma sheath around the antenna. With the ion dynamics neglected, the antenna is charged completely negatively so that no more electrons in the plasma can reach the antenna after the formation of the sheath. When the ion dynamics are included, the electrons impulsively impinge upon the antenna while the ions reach the antenna in a continuous manner. In such a case, the antenna charge density and electric field have a brief excursion of slightly positive values during which there is an electron sheath. The electron and ion currents collected by the antenna are weak and balance each other over each oscillation cycle. The sheath–plasma boundary is a transition layer with fine structures in electron density, charge density, and electric field distributions. The sheath radius oscillates at the antenna current frequency. The calculated antenna reactance is improved from the theoretical value by 10%, demonstrating the advantage of including the plasma sheath effects self-consistently using the PIC simulations. The sheath tends to shield the electric field from penetrating into the plasma. There is, however, leakage of an electric field component with significant amplitude into the plasma, implying the applicability of the high-voltage antennas in whistler wave transmission in the inner magnetosphere.

Citation: Tu, J., P. Song, and B. W. Reinisch (2008), Plasma sheath structures around a radio frequency antenna, *J. Geophys. Res.*, *113*, A07223, doi:10.1029/2008JA013097.

1. Introduction

[2] When an actively transmitting antenna is immersed in a plasma, the particle distributions around the antenna are greatly disturbed because of the electromagnetic field excited by the antenna and/or the current collection by the antenna. In the presence of such antenna–plasma interaction several situations can arise. For a receiving antenna, there is a region of low electron density (ion plasma sheath) when the antenna is in an equilibrium plasma [e.g., *Morin and Balmain*, 1993] or a region of high electron density (electron plasma sheath) when there are photoelectron emissions from the antenna surface [e.g., *Tsutsui et al.*, 1997; *Zhao et al.*, 1996]. In the case of a VLF wave transmission antenna, there may be an ion sheath in the vicinity of the antenna because of the large difference in the timescales of the ions and electrons with which the ions and electrons respond to the varying electromagnetic field transmitted by the antenna. The plasma sheaths act to modify the antenna impedance and thus change characteristics of the electromagnetic wave transmission from the antenna. This is particularly true when the antenna is driven by a high-voltage source so that the size of the sheath is large [*Shkarofsky*, 1972]. It is necessary to study the interactions between the high-voltage antenna and plasma because of the potential application of a high-voltage whistler wave transmitter in controlled precipitation of the radiation belt electrons [*Inan et al.*, 2003].

[3] In the past 50 years, extensive studies have been conducted to understand the impedance properties of the antennas in plasma, treating the plasma around the antennas as a medium with given constant dielectric tensor [e.g., *Balmain*, 1964; *Kuehl*, 1966; *Nakatani and Kuehl*, 1976; *Nikitin and Swenson*, 2001]. In a recent simulation study, *Ward et al.* [2005] developed a finite difference time domain (FDTD) model to investigate the impedance of a short

[1]Center for Atmospheric Research, University of Massachusetts, Lowell, Massachusetts, USA.
[2]Environmental, Earth, and Atmospheric Sciences Department, University of Massachusetts, Lowell, Massachusetts, USA.

0148-0227/08/2008JA013097

dipole antenna in a magnetized plasma. In the work of *Ward et al.* [2005] the plasma was treated as a multicomponent fluid with the electron density and velocity varying in response to the electromagnetic field excited by the transmitting antenna. Their study revealed that the antenna current distribution deviates significantly from the triangular distribution near the fundamental plasma frequencies. However, the sheath effects were not included due to the large and disparate temporal scale of the sheath compared to the upper hybrid oscillation period [*Ward et al.*, 2005].

[4] A number of early works have included the plasma sheath effects in investigations of the antenna impedance [e.g., *Mlodnosky and Garriott*, 1963; *Shkarofsky*, 1972; *Baker et al.*, 1973]. However, the physics of the antenna–plasma interaction, particularly in the case of the high-voltage antennas, has not been well understood. Thus the effects of the plasma sheath, represented by an additional impedance due to the sheath, were introduced based on predefined sheath models. Those sheath models are essentially electrostatic and are resulted from the boundary conditions that both electric field and potential are zero at the plasma sheath edge [e.g., *Riemann*, 1991 and references therein]. Such boundary conditions may not be valid in the case of transmitting antenna, especially for the case of a high-voltage source [*Song et al.*, 2007]. Adopting such predefined sheath models may be one of the reasons that the theoretical values of the sheath capacitance predicated by, e.g., *Shkarofsky* [1972], were an order of magnitude smaller than the measured ones, as revealed by the experiment–theory comparison made by *Oliver et al.* [1973].

[5] Recently *Song et al.* [2007] proposed an improved model to evaluate the impedance of a high-voltage antenna in the frequency range of whistler waves. In this new model, a bare metal antenna is assumed to be charged to a negative potential based on physical arguments. The plasma sheath (an ion sheath) is formed to satisfy the boundary conditions on the antenna surface, as well as at the plasma sheath boundary where the electric potential is not zero. It is also assumed that the sheath is free of electrons and conduction current when the transmission frequency is much higher than the ion characteristic frequencies but significantly below the electron characteristic frequencies. The sheath–plasma boundary is simply treated with a step function and is defined at the location within which the net charge on the antenna and in the sheath is zero. The radius of this boundary, or the sheath radius, varies in response to the oscillations of the charge/voltage on the antenna. The oscillating sheath radius translates to a current in the surrounding plasma, which radiates waves into the plasma. Compared to the whistler wave transmission experiment conducted using the radio plasma imager (RPI) instrument on the IMAGE satellite [*Reinisch et al.*, 2000], the model describes some important physical processes occurring in the high-voltage antenna–plasma interaction. The sheath capacitance predicted by *Song et al.* [2007] is about 20% lower than that from the RPI experiment, a significant improvement over the previous theoretical studies.

[6] The model by *Song et al.* [2007] treated only the steady-state transmission without self-consistent introduction of the plasma sheath formation and initial antenna charging process. More importantly, the ion dynamics are ignored by assuming a transmission frequency much higher than the ion characteristic frequencies. The effects of the ion dynamics, however, may be substantial since the frequency of the whistler wave to be transmitted is likely not much higher than the ion characteristics frequencies. For instance, in the plasmasphere the electron gyrofrequency is significantly lower than the electron plasma frequency, leading to a condition in which the whistler wave frequencies are only few times of the ion plasma frequency.

[7] In this paper we for the first time use a particle-in-cell (PIC) simulation code to self-consistently investigate the antenna–plasma interactions for a high-voltage antenna in space plasma. The simulations allow detailed examination of the antenna charging processes and plasma sheath structures that are difficult to tackle analytically. In addition, the simulations can incorporate effects of the ion dynamics on the antenna charging and plasma sheath structures. The simulation results provide new insights to the physical processes occurring in the antenna–plasma interaction in the frequency range below the electron plasma frequency, especially for the case including the ion dynamics. We discuss the numerical simulation model in the next section and present the simulation results for the case without ion dynamics in section 3. The results from the simulation with ion dynamics included are presented in section 4. The final section gives a summary with discussions.

2. Simulation Model

2.1. Numerical Scheme

[8] In this study we consider an electrically short dipole antenna driven by a high-voltage source, as schematically displayed in Figure 1. We consider a cylindrical bare antenna that is perfectly conducting. The antenna is long compared to its thickness and the radial scale of the sheath. We use a cylindrical coordinate system (r, ϕ, z) that has its z axis coincide with the axis of the thin cylindrical antenna and the coordinate origin at the center of the dipole antenna as shown in Figure 1.

[9] As a first step toward developing a comprehensive kinetic simulation model for studying the antenna–plasma interaction, in the present study we adopt some approximations used by the theoretical analysis of *Song et al.* [2007]. These approximations include weak effects of the magnetic field compared to the electric field induced by the high-voltage source, cold plasma, and negligible end effects at the antenna tips. However, we do not predefine the electron density distribution surrounding the antenna during its time evolution, as *Song et al.* [2007] did, but allow the electron and ion density to vary in response to the electric field force that is self-consistently calculated. As a result, the plasma sheath will be self-consistently formed. We perform simulations with both immobile and mobile ions so that we can examine effects of the ion dynamics, which are excluded by the study of *Song et al.* [2007] study. *Song et al.* [2007] have argued that as long as the antenna is not extremely thin, say less than 0.01 m in radius, the magnetic field effects produced by the antenna driving current can be neglected in a zeroth-order treatment. This is because the magnetic force term in momentum equation and magnetic field term in Faraday's law are much weaker than the corresponding electric field terms in the case of high-voltage antennas. Adopting this approximation means that

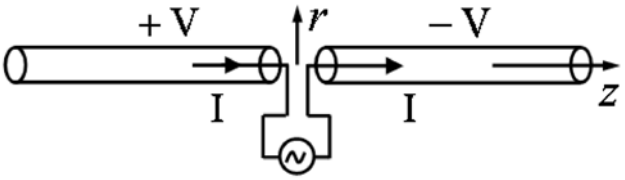

Figure 1. Schematic display of a short dipole antenna system. Arrows indicate the current at a time corresponding to the polarity of the antenna. The r and z axes of the cylindrical coordinates are shown.

we perform quasi-electrostatic simulations in the present study. Neglecting the end effects excludes the z component (in the antenna orientation) of the electric field, which may cause some errors. Nevertheless, this electric field component probably extends only in a distance comparable to the sheath size. Furthermore, the plasma thermal energy is much smaller than the kinetic energy once the charged particles are accelerated by the strong electric field of the transmission voltage, which justifies the cold plasma approximation.

[10] It should be pointed out that in the present simulations the background magnetic field is also excluded, making the plasma isotropic (unmagnetized). Therefore, at the frequency considered there will be actually no electromagnetic wave transmission from the antenna in a cold plasma. This means the present simulations cannot deal directly with the effects of the plasma sheath on the wave transmission. Nevertheless, such simulations can reveal the detail structures of the plasma sheath and provide insights to the physical processes occurring in the antenna–plasma interaction for the high-voltage antenna. The presence of a background magnetic field will alter the plasma sheath structures, e.g., the sheath may show some degrees of asymmetry with respect to the background magnetic field. The alteration of the plasma sheath by the background magnetic field, however, may be slight because the plasma sheath structures are predominantly controlled by the very strong electric field in the vicinity of the high-voltage antenna. Note that the situation we consider here is different from the spacecraft charging in which the electric field is weak and the effects of the geomagnetic field is significant [e.g., *Laframboise and Sonmor*, 1993].

[11] For an electrically short antenna the antenna current, driven by a voltage source and flowing on the antenna surface, can be approximated as a triangular distribution [e.g., *Balmain*, 1964].

$$I_A = I_0(1 - |z|/l)e^{j(\omega t+\delta)},\ -l \le z \le l \tag{1}$$

where l is the length of each branch of the antenna, ω is the angular frequency of the antenna current, and δ is the initial phase of the current relative to the driving voltage. This approximation is valid as long as the transmission frequency is not close to the fundamental plasma frequencies [*Ward et al.*, 2005]. The antenna current is the largest at the feeding point of the each branch of the antenna (neglecting the gap between two branches of the antenna) $z = 0$, and zero at the antenna tips $z = \pm l$. The charge on the antenna surface is uniformly distributed along the antenna according to the charge conservation for such a linear distribution of the current. The electric field on the antenna surface is thus perpendicular to the antenna surface except at the antenna tips and in the gap between the feeding points of the two branches of the antenna. If the end effects at the antenna tips and in the gap of the two branches are neglected, all the physical parameters, except the antenna current, do not vary along the z coordinate. Plus the azimuthal symmetry, the problem to be solved becomes 1D. Neglecting the end effects is a crude approximation, particularly in the gap of the two antenna branches, and may be an important cause of the difference between theoretical value of the antenna capacitance by *Song et al.* [2007] and that from the RPI experiments.

[12] With above approximations adopted, the simulation model solves the time-dependent, 1D electric field through Gauss's law

$$\frac{\partial E_r}{\partial r} = \frac{\rho}{\epsilon_0} \tag{2}$$

where E_r is the component of the electric field perpendicular to z axis, ρ is charge density and ϵ_0 is vacuum permittivity. The electron and ion simulation particles (or superparticles), which represent a number of real electrons and ions, respectively [*Hockney and Eastwood*, 1988], are advanced through equations of motion, after neglecting the weak Lorentz force

$$\frac{d\gamma_s m_s v_s}{dt} = q_s E_r \tag{3}$$

where m_s is the mass of a simulation particle of species s in the rest frame, v_s and q_s are the velocity component in r direction and charge of the particle, respectively, $\gamma_s = 1/\sqrt{1-(v_s/c)^2}$, and c is the speed of light in vacuum. With symmetry about the z axis, the electric field has only an E_r component, and particles move only in the r direction when the magnetic field is neglected.

[13] The spatial domain is from r_0 to maximum radial distance r_m, where r_0 is the radius of a cylindrical antenna. The spatial domain is divided into m cells, and N_s pairs of simulation electrons and ions are initially loaded with a uniform number density n_0. At each time step the charge density distribution ρ_j on the cell grids r_j ($j = 0, 1, 2, \ldots, m$) is calculated with linear weighting. That is, for particles located in the cell $[r_j, r_{j+1}]$, the part of the charge assigned to grid j is given by [*Birdsall and Langdon*, 1983]

$$Q_j = \sum_{s,i} q_s \frac{r_{j+1}^2 - r_i^2}{r_{j+1}^2 - r_j^2} \tag{4}$$

and the part assigned to $j + 1$ is

$$Q_{j+1} = \sum_{s,i} q_s \frac{r_i^2 - r_j^2}{r_{j+1}^2 - r_j^2} \tag{5}$$

where r_i is the particle location, q_s is the charge of the particle in unit length along z axis, and summation is over

all species and all particles of each species in the cell. The electric fields on the grids are then calculated by integrating Gauss's law

$$2\pi r_{j+1}E_{j+1} - 2\pi r_j E_j = \frac{Q_j + Q_{j+1}}{2\epsilon_0} \tag{6}$$

where Q_j represents the charge (not charge density) in unit length along z axis assigned onto the grid j.

[14] The simulation particles represent a number of real particles [*Hockney and Eastwood*, 1988]. This number, referred to as the weight of the simulation particles, is determined by the number of simulation particles of each species, the size of the simulation spatial domain, number of cells, and the initial density of the species. At each time $t = n\Delta t$ (Δt is time step), the simulation particles are advanced using a leapfrog algorithm [*Birdsall and Langdon*, 1983]

$$(\gamma_s v_s)^{n+1/2} = (\gamma_s v_s)^{n-1/2} + \left(\frac{q_s E_{ri}}{m_s}\right)^n \Delta t \tag{7}$$

$$r_i^{n+1} = r_i^n + v_s^{n+1/2}\Delta t \tag{8}$$

where E_{ri} is the electric field acting on the particle at location r_i (within cell $[r_j, r_{j+1}]$) at $t = n\Delta t$. The superscript n in equations (7) and (8) denotes values at nth time step, and $n + 1/2$ indicates at a half time step (between $n\Delta t$ and $(n + 1)\Delta t$). Since the electric fields, E_j, solved from equation (6), are located on the spatial grids, the electric field E_{ri} must be interpolated from E_j ($j = 0, 1, 2, \ldots, m$). We apply the same linear weighting for charge assignment to calculate E_{ri} from the electric fields at r_j and r_{j+1} in order to conserve particles' momentum [*Birdsall and Langdon*, 1983; *Hockney and Eastwood*, 1988]. With the leapfrog algorithm, $(\gamma_s v_s)$ is advanced from $t = (n - 1/2)\ \Delta t$ to $t = (n + 1/2)\ \Delta t$, while the particle location r_i is advanced from $t = n\Delta t$ to $t = (n + 1)\ \Delta t$. Thus we need $(\gamma_s v_s)$ and velocity v_s at $t = -(1/2)\ \Delta t$, which are calculated by pushing $(\gamma_s v_s)$ and v_s at $t = 0$ back to $t = -(1/2)\ \Delta t$ using the electric field at $t = 0$ and initial (at $t = 0$) velocity v_s.

2.2. Boundary Conditions

[15] Boundary conditions, for both the electromagnetic fields and particles, have crucial influences on the particle simulation results [*Dum*, 1984]. In the present study, the simulation domain is from r_0 (inner boundary, on the antenna surface) to r_m (outer boundary). The boundary condition for the electric field at r_0 (on the surface of the bare antenna) is dictated by the surface charge density on the antenna, σ_A, i.e.,

$$E_A = E_r(r_0) = \frac{\sigma_A}{\epsilon_0} \tag{9}$$

for a perfectly conducting antenna.

[16] The antenna surface charge density includes the contribution from both the antenna current and the charged particles that impinge and reside on the antenna surface. Because of the azimuthal symmetry, the antenna surface charge density due to the antenna current is obtained by integrating the charge conservation equation over the antenna cross-section. Using the antenna current distribution of equation (1), we obtain for one of the antenna branches

$$\sigma_{ai} = \frac{I_0}{2\pi\omega r_0 l} e^{j(\omega t + \delta + 3\pi/2)} \tag{10}$$

Equation (10) (taking the real part of the right hand side) is used to calculate the oscillating charge density on the antenna surface. The collected charge density, σ_c, from the contribution of the charged particle bombardment onto the antenna is obtained by collecting the particles that reach the antenna surface from $t = 0$ to the current time step. The total charge density on the antenna surface at the current time step is then $\sigma_A = \sigma_{ai} + \sigma_c$, which is used in equation (9) to determine the electric field on the antenna surface. According to Gauss's law the electric field on any grid r_j is determined by the charge enclosed within the circle of a radius r_j (see equation (6)). The electric field at the outer boundary $r = r_m$ can be calculated from equation (6) when the charges on grids r_j ($j = 0, 1, 2, \ldots, m$) are known. Therefore we do not need an outer boundary condition for the electric field. However, we need a boundary condition for charge Q_m at the outermost grid r_m.

[17] The specification of Q_m at r_m appears to be difficult. From equations (4) and (5), we see that the charge Q_m at the outer boundary r_m includes the contribution of the particles in both cell m and those outside the outer boundary. Since the locations of those particles outside the simulation domain are unknown, Q_m cannot be fully determined. Therefore, at each time step, we approximate Q_m by Lagrangian extrapolation of the charges Q_j ($j = 0, 1, 2, \ldots, m - 1$) to r_m. Note that the evaluation of charges assigned to all grids are done after the particle removal at the inner boundary r_0 and particle injections at the outer boundary r_m described in the following subsection.

2.3. Particle Removal and Injections

[18] The simulation particles may move outside the simulation box because of either hitting the antenna surface at $r = r_0$ or moving beyond $r = r_m$. Those particles are removed from the active particle list in the simulation domain. The charges of the particles that hit the antenna are collected and included as the antenna surface charge. At the outer boundary r_m, particles may inject into the simulation domain from the outside. However, we do not have a priori knowledge to determine the velocities of the injected particles and their locations in the simulation domain. Such a difficulty arises from the fact that we only can simulate a limited portion of the plasma and that the electric fields beyond the outer boundary are unknown. In the case of a high-voltage antenna, the electric fields beyond the outer boundary are significant and their effects on the particles outside the simulation domain are not negligible when considering the particle injections. The particle injections at the outer boundary thus have to be treated approximately. In the present simulations, we treat the particle injections at the outer boundary with the following method.

[19] First of all we notice that the total current (conduction plus displacement current) in the plasma is independent

of r in the 1D problem that only has r dependence. From the divergence of Ampere's law

$$\nabla \cdot \nabla \times \mathbf{B} \equiv 0 = \nabla \cdot \left(\mu_0 \mathbf{J} + \epsilon_0 \mu_0 \frac{\partial \mathbf{E}}{\partial t} \right) \tag{11}$$

where $\mathbf{B}$ is magnetic field, $\mathbf{J}$ is conduction current density, and μ_0 is vacuum susceptibility, we have that the sum of the conduction and displacement current is independent of r

$$I_{total}(r,t) = I(r,t) + 2\pi r \epsilon_0 \frac{\partial E(r,t)}{\partial t} = \text{const.} \tag{12}$$

where $I(r, t) = 2\pi r J(r, t)$ is the conduction current flowing through the cylindrical surface of radius r with unit length in the z direction. Because of condition (12), the total current evaluated at the grid r_m should be equal to that at the grid r_{m-1}, i.e., $I_{total}(r_m, t) = I_{total}(r_{m-1}, t)$ at any given time. An imbalance between $I_{total}(r_m, t)$ and $I_{total}(r_{m-1}, t)$ indicates that a number of electrons or ions should be injected into the simulation domain because the total current is equivalent to the charges passing through the cylindrical surface in unit time. Specifically, the number of particles to be injected at any time step is given by

$$N_{inj} = (I_{total}(r_m, t) - I_{total}(r_{m-1}, t))(\Delta t / q_s) \tag{13}$$

If $I_{\text{total}}(r_m, t) < I_{\text{total}}(r_{m-1}, t)$, N_{inj} is the number of electrons (then q_s is the electron charge) to be injected to compensate for the larger current flowing through cylindrical surface of radius $r = r_{m-1}$. Otherwise, N_{inj} is the number of ions to be injected.

[20] As mentioned previously, there is no precise way to determine the velocities and the locations of the injected particles. The procedure adopted in the present simulations is that at each time step the velocities of the injected particles are calculated using the electric field at the outer boundary and then multiplied by a random number in the range of 0–1

$$\gamma_s v_s = -|q_s E(r_m)/m_s| \Delta t \, \text{rand}() \tag{14}$$

The injected particles are then calculated using

$$r_i = r_{m-1} + v_s \Delta t \, \text{rand}() \tag{15}$$

[21] We have tested several different methods of the particle injection and specification of Qm. For example, we have set the velocities of the injected particles to zero with their locations randomly distributed in cell m, and used linear extrapolation of the charges inside the outer boundary to specify Q_m. It is found that the simulation results in 12 oscillating periods are essentially the same for the different methods we have tested, suggesting that the effects of the particle injections and the outer boundary condition for the charge distribution propagate only slowly inward.

[22] Randomly assigning velocities to the injected particles introduces an effective temperature to the electrons and ions. We note that the amplitude of the electric field at the outer boundary is about 1 V/m, as will be shown by the simulation results. Using 1 V/m in equation (14) and values for charge, mass, and time step ($\Delta t = \sim 8.3 \times 10^{-8}$ s) introduced in section 3, the energies assigned to the injected electrons and ions are in the range of $0 - 6 \times 10^{-4}$ eV and $0 - 3 \times 10^{-7}$ eV, respectively. Taking the energy spread as the measure of the temperature, the effective temperatures of the electrons and ions are thus about 6×10^{-4} eV and 3×10^{-7} eV, respectively, which are very low. Therefore the randomness in injecting the particles essentially does not lead to a warm plasma in the simulation domain.

2.4. Initial Conditions

[23] At $t = 0$ the simulation electrons and ions are loaded into the simulation box with a uniform density. Initially individual pairs of electron and ion are placed at the same location so that the charge density in the simulation domain is zero at $t = 0$. The initial electric field distribution is determined by the surface charge on the antenna surface at $t = 0$, using equations (6) and (9). The velocities of the electrons and ions at $t = 0$ are set to zero. The leapfrog algorithm requires that initial velocities of the electrons and ions (if ions are mobile in the simulation) are set at $t = -(1/2)\,\Delta t$, which are calculated using equation (3) with one half time step backward.

3. Simulation Results With Immobile Ions

[24] In this section we describe the simulation results when the ions are assumed as fixed background of the positive charge. We use the following parameter values for the simulations. The antenna radius is $r_0 = 0.2$ m and simulation domain expands to $r_m = 200.2$ m. This simulation domain is divided into $m = 1000$ cells uniformly and thus the spatial resolution is $\Delta r = 0.2$ m. The initial electron and ion densities are set to be uniform with a value of $n_0 = 500$ cm^{-3} (5×10^8 m^{-3}). Initially 2.5×10^7 pairs of simulation electrons and ions are loaded into the simulation domain, with their velocities and temperatures set to be zero. The number of the simulation particles in cell 1 is smallest because it is the cell with smallest area: there are 75 simulation electrons and 75 simulation ions initially. The number of simulation particles increases in the cells further away from the antenna. The weight of the simulation particles (the number of real particles represented by a simulation particle) is $w = \sim 2.51 \times 10^6$. The charge of a simulation electron and ion is $\mp 1.6 \times 10^{-19} w$ Coulomb, respectively. The mass of a simulation ion is $1.67 \times 10^{-27} w$ kg while the mass of a simulation electron is $9.1 \times 10^{-31} w$ kg. The mass ratio of ion to electron is thus 1843 (real mass ratio). The real mass ratio is used to avoid difficulty in scaling simulation parameters to physical quantities (one of our objectives, for example, is to know physically how large the plasma sheath radius is). The time step is set as $\omega_p \, \Delta t = 0.1047197$, where $\omega_p^2 = \omega_{pe}^2 + \omega_{pi}^2$, ω_{pe} and ω_{pi} are electron and ion plasma frequency in rad/s, respectively. The length of each antenna branch is 100 m. The amplitude of the antenna current at $z = 0$, driven by the high-voltage source, is $I_{a0} = 0.4$ A, and the oscillating frequency of the current is $f = 30$ kHz, which is lower than the electron plasma frequency $f_{pe} \approx 200.64$ kHz but higher than the ion plasma frequency $f_{pi} \approx 4.68$ kHz. The simulation focuses on one branch of the antenna (another branch is 180° out of phase). The initial phase of the current is set

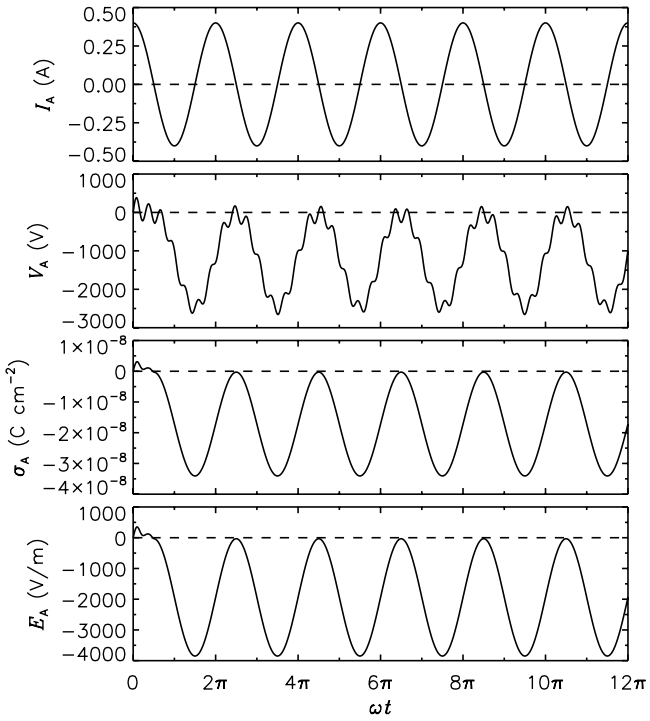

Figure 2. Time variations of the antenna current (input current to the antenna), antenna potential, antenna surface charge density, and normal electric field on the antenna surface (first to last panels) from the simulation neglecting the ion dynamics.

to $\delta = 0$ (the initial phase of the current on another antenna branch is $\delta + 180°$). It should be pointed out that using different values of δ does not affect the simulated physical processes. We conduct simulations at only one frequency because the emphasis of the present study is to reveal the physical processes occurring in the antenna–plasma interaction for the high-voltage–driven antenna.

3.1. Antenna Charging and Impedance

[25] We first examine the antenna charging process in the simulation with the ion dynamics ignored. In Figure 2 we display, from the first to the last panels, the time variations of the antenna current (at the antenna feed point), the electric potential on the antenna surface, the surface charge density, and the normal electric field on the antenna surface. Note that the electric field, potential, and the charge density on the antenna surface are uniformly distributed along the antenna on the basis of 1D assumption. The potential reference position is set at r_m. It is seen that the antenna charging occurs in a transit dynamic process, and is completed in about one-fourth of an antenna current oscillation period because of the fast response of the light electrons. Without negative charging the antenna charge density should keep on increasing to reach its maximum value at one-fourth cycle. After negatively charged, the antenna surface charge density σ_A oscillates steadily, varying between about -2.87×10^{-10} C cm^{-2} and -3.41×10^{-8} C cm^{-2}, while the electric field on the antenna surface oscillates between about -3848.6 V/m and -32.4 V/m. The maximum value of the electric field is less than zero (-32.4 V/m). This is because the antenna is overly charged: the maximum antenna surface charge density is less than zero. We will discuss this issue later when discussing the causes of the antenna charging. The oscillation frequency of both antenna surface charge density and electric field is 30 kHz, the same as that of the antenna driving current. The antenna potential essentially lies below zero because of the charging and also oscillates at the antenna current frequency. The slight positive value of the antenna potential are due to the arbitrary selection of the potential reference point at the outer boundary. The potential there may actually not be zero with respect to the potential of the ambient plasma. The DC voltage associated with the antenna charging is about -1225.7 V.

[26] Figure 2 shows that the phase of the antenna current is nearly 90° in advance of the antenna potential, indicating that the antenna impedance is mainly capacitive. The phase difference between the antenna potential and current, averaged over 6 oscillating cycles, is about $-88.59°$. From the relationship between the antenna potential and current, we can calculate the antenna reactance X_s. The potential (relative to the reference point at $r_m = 0$) of the other antenna branch is 180° out of phase, and the potential difference (or voltage) between the two antenna branches is just the potential shown in Figure 2 with the DC component removed. The peak-to-peak potential difference, averaged for 6 oscillating periods shown in Figure 2, is 2789.8 V. The peak-to-peak antenna current is 0.8 A. The antenna reactance is thus calculated to be $X_s = -3486.2\ \Omega$. Compared to that given by equation (29) in the study by *Song et al.* [2007] ($X_s = -3175\ \Omega$) using the same parameter values, the reactance from the simulation is about 10% larger than that from the theoretical model. This is an improvement from the analytical value but still underestimates the IMAGE RPI experiment value by about 10%.

[27] The antenna charging is caused by the electrons in the plasma that attach to the surface of the antenna, as shown by Figure 3, which displays the time history of the number of electrons that are attracted onto the antenna. Within the first one-fourth of an oscillating period, there are a large number of electrons reaching the antenna. After that short period, no more electrons can reach the antenna surface because of the negative antenna surface charge density, and hence the negative (directed toward the antenna) electric field on and near the antenna surface. Note that the antenna charging does not stop at the time when the antenna surface charge σ_A density becomes zero. Instead, it stops when σ_A becomes negative (-2.87×10^{-10} C cm^{-2}). The reason for extra charging is that some electrons in the plasma, which are accelerated toward the antenna, have finite kinetic energies to overcome the negative potential and reach the antenna. Only when the negative charge density on the antenna is large enough (in value), all the electrons, including those that have been accelerated toward the antenna, can no longer reach the antenna. It will be shown later that when the ion motion is allowed the antenna will not be completely charged to negative charge density through a whole oscillation cycle.

3.2. Plasma Sheath Structures

[28] After the antenna is negatively charged, the antenna surface electric field becomes negative. This negative electric field repels electrons away from the proximity of the antenna, leaving a region with extra ions (positive charges). This region is an ion sheath, which is observed in the

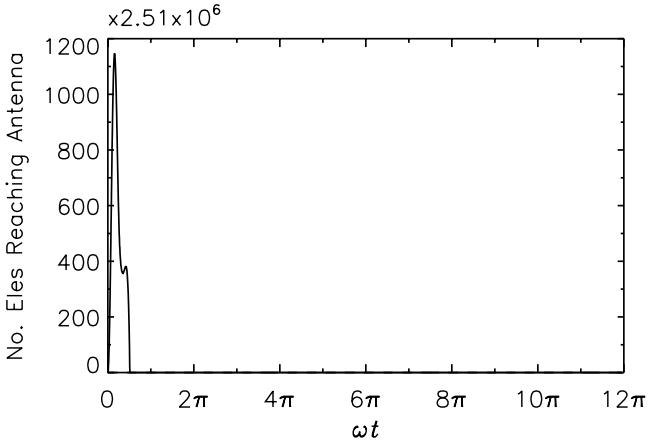

Figure 3. Number of electrons that reach the antenna from the surrounding plasma as a function of time.

electron and charge density distributions at individual time steps. Figure 4, which displays sample snapshots of the electron density distribution and the charge density distribution at ωt = 34.31 (dashed line) and ωt = 36.62 (solid line), clearly shows the ion sheath and its spatial structures. Around the antenna is a region where the electron density is greatly depleted (essentially zero, see top panel) and the background ions provide a constant positive charge density of 8×10^{-17} C cm^{-3} (see the bottom panel). Outside the sheath, the electron density remains around its initial value of 500 cm^{-3} with fluctuations of small amplitudes because of the limited number of simulation particles. The boundary from the ion sheath to the plasma (hereafter we refer to it the sheath–plasma boundary) is a transition region with a finite length of about 7 m. Both the electron and charge densities have sharp gradients at the inner edge of the sheath–plasma boundary so that the step function description of the electron and charge density is a very good approximation [*Song et al.*, 2007], if the fine structures of the electron and charge density in the transition region are neglected. Immediately away from the sharp gradient, the electron density at ωt = 36.62 shows an overshoot and then gradually returns to 500 cm^{-3}. Correspondingly, the charge density in the same region is negative and then keeps essentially zero further away from the sheath. The electron density enhancement is

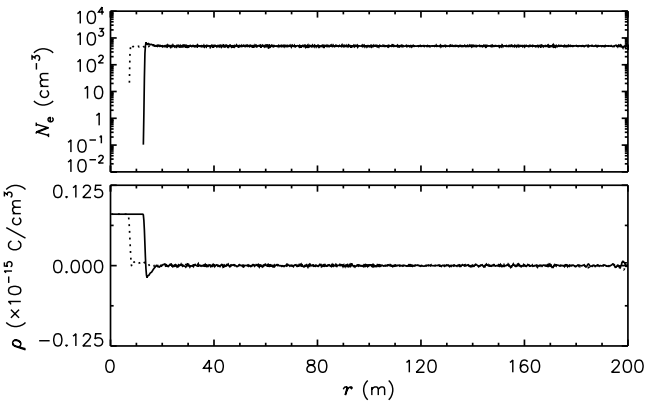

Figure 4. Electron density distribution (top panel) and charge density distribution (bottom panel) at ωt = 34.31 (dashed line) and ωt = 36.62 (solid line).

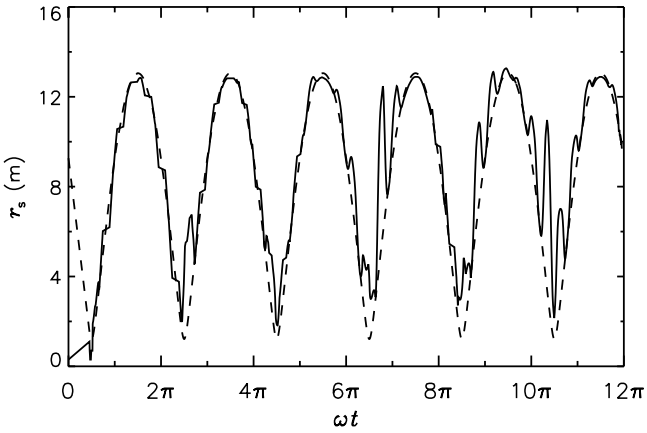

Figure 5. Oscillations of the radius of the sheath–plasma boundary. The dashed line is the time variation of the sheath–plasma boundary calculated using the theoretical model of *Song et al.* [2007].

due to a pileup of electrons in the transition layer at this time. Note that the electric fields in the sheath always direct toward the antenna (negative values) even though the electric fields oscillate at the frequency of the antenna current. The electric field in the transition region and in the plasma, on the other hand, primarily oscillates at the plasma frequency and has positive and negative phases, as will be shown in Figure 7. The pileup occurs when the electric field in the transition region is in its negative phase, e.g., at ωt = 36.62 (corresponding to the second vertical dashed line in Figure 7). The electrons at the inner edge of the boundary are strongly pushed outward by the stronger electric field in the transition region while the electrons further away experience much weaker electric field force. When the electric field in the transition region is in its positive phase, e.g., at ωt = 34.31 (first vertical dashed line in Figure 7), the electron density overshoot almost disappears. The transition region, which has been neglected in the analytical treatment of *Song et al.* [2007], may be one of the causes of the small difference in the antenna reactance between the simulated and theoretical values.

[29] The sheath size, or the sheath radius in a cylindrical case, oscillates with the antenna current frequency as can be seen in Figure 5, which displays the time variation of the sheath–plasma boundary radius r_s. The boundary is defined at where the charge enclosed inside the boundary is equal (but with opposite sign) to that on the antenna surface, in unit length in the z direction. The dashed line represents the sheath–plasma boundary variation calculated using equation (21) in the study of *Song et al.* [2007]. In calculating the theoretical values of r_s, the antenna surface charge density from the simulation is used to evaluate the static sheath radius in equation (17) in the study of *Song et al.* [2007] because the antenna surface charge density is not calculated in the theoretical model. The spikes in the simulated boundary radius are caused by the noise in the charge density, which sometimes results in the fluctuations in determining the boundary location. It is found that the simulated sheath–plasma boundary radius is in good agreement with the theoretical values when the antenna surface charge density from the simulation is used. Both oscillate at

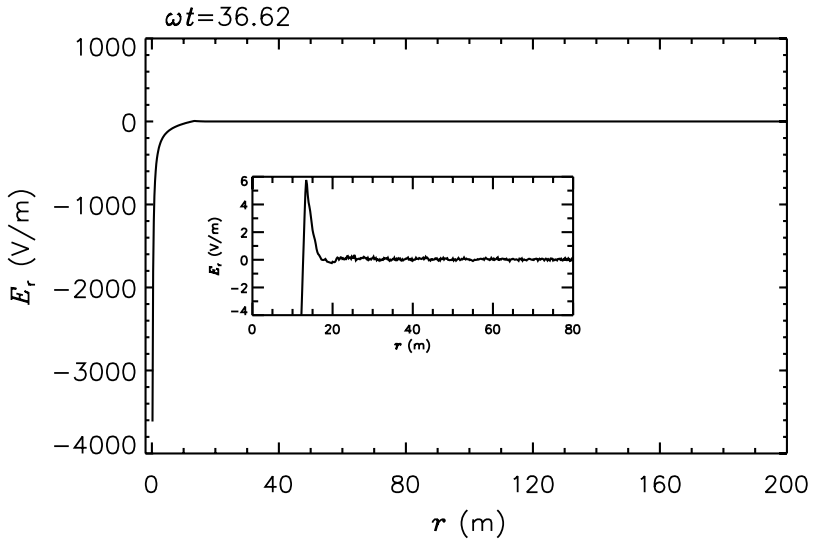

Figure 6. The electric field distribution at $\omega t = 36.62$. The inserted figure displays fine structures of the electric field around the sheath–plasma boundary at this time.

the antenna current frequency. It is also interesting to note that once formed the sheath region maintains a minimum radius above 1.5 m. It never shrinks to the antenna surface during its oscillations. This is because the antenna is negatively charged and the electric field near the antenna is always negative. Note that the theoretical formula for r_s is valid only after the antenna charging process is completed. The theoretical values, therefore, are different from the simulated within the first one-fourth oscillating period when the antenna charging is ongoing.

3.3. Electric Shielding by Plasma Sheath

[30] The plasma sheath acts as a shield to the antenna electric field so that it is expected that the electric field is significantly weaker outside the sheath. This is indeed the case by examining the spatial distribution of the electric field at all time steps. As an example, we show in Figure 6 the spatial distribution of the electric field at $\omega t = 36.62$. It is seen that there is a very strong electric field in the sheath region, but a much weaker electric field outside. The inserted panel on Figure 6 reveals the fine structure of the electric field around the sheath–plasma boundary. A positive spike at the inner edge of the sheath–plasma boundary layer is observed followed by a weak negative excursion, which are the electric field structures of the transition region. The positive spike can be explained by the charge density distribution shown in Figure 4 also for the time moment of $\omega t = 36.62$. The charge density inside the sheath is positive, which tends to weaken the strength of the negative electric field when moving away from the antenna. Thus the electric field increases rapidly to positive values at the inner edge of the boundary layer. The charge density then suddenly drops to negative values because of the pileup of the electrons in the transition layer as discussed in the previous subsection. Therefore the electric field rapidly decreases, forming a spike in the transition layer.

[31] It is also interesting to examine the time variations of the electric field. In Figure 7, we show the time variation of the electric field at three different locations: inside the sheath close to the antenna at $r = 0.3$ m; around the sheath–plasma boundary at $r = 12.1$ m; and far away from the sheath at $r = 36.1$ m. Since the minimum sheath radius is above 1.5 m, the location $r = 0.3$ m is always inside the sheath. The electric field in the sheath is strong and oscillates with the antenna current frequency because the sheath region is free of electrons and the ions are fixed (thus no oscillating charges inside the minimum sheath radius of $r_s < \sim 1.5$ m). At $r = 12.1$ m, which is close to the maximum radius ($\sim$13.5 m) of the sheath–plasma boundary, the electric field either primarily oscillates with the plasma frequency when the sheath–plasma boundary is within $r = 12.1$ m or has a stronger amplitude and varies with the antenna current frequency when the sheath–plasma boundary is outside $r = 12.1$ m. Away from the maximum radius of the sheath–plasma boundary, the electric field primarily oscillates at the plasma frequency but modulated by the antenna current frequency.

[32] The plasma oscillations are caused by the penetration of the electric field into the plasma before the plasma sheath is formed. In the simulation, the penetrated electric field perturbs the electrons and causes the electron plasma oscillations. The sheath acts to shield the antenna electric field, as discussed before. However, such shielding is not perfect. Therefore the antenna electric field, which oscillates at the antenna current frequency, can leak into the plasma even after the sheath is formed. This component at the antenna current frequency modulates the plasma oscillations as seen in Figure 7. It is noted that in the present simulation there is no transmitted wave since we actually considered an unmagnetized cold plasma. In the unmagnetized cold plasma the waves that can propagate must have a frequency higher than the plasma frequency. Note that we have argued that the random injection of the particles from the outside of the simulation domain does not introduce substantial warm plasma.

[33] Although the electric field beyond the sheath–plasma boundary is weak compared to that in the sheath, its oscillating amplitude is significant. The electric field beyond the sheath primarily oscillates at the plasma frequency but modulated by the antenna current frequency. The amplitude of this modulated component is around

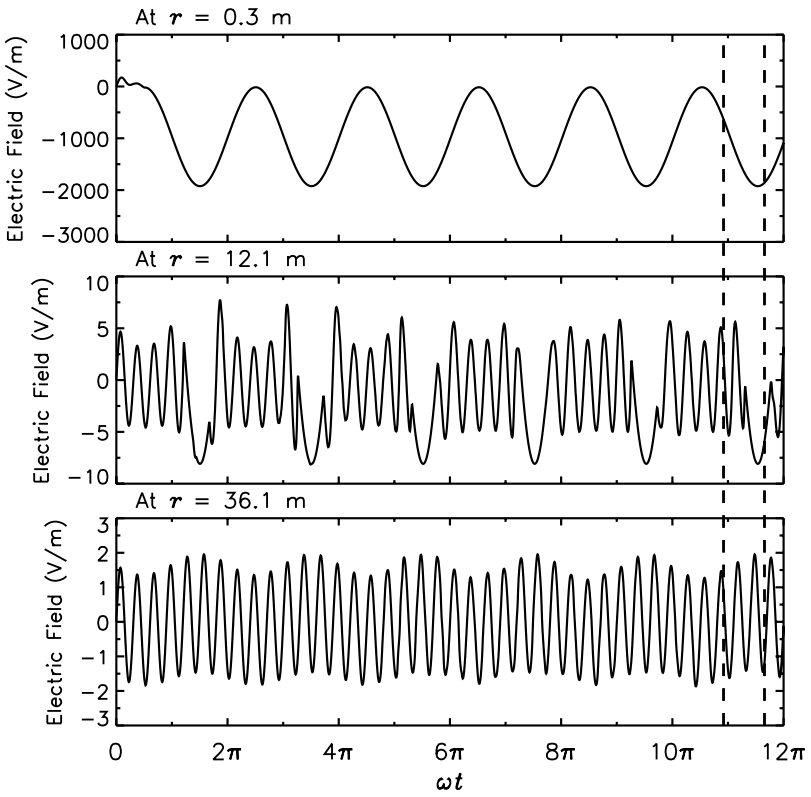

Figure 7. Time variation of the electric field at three selected locations as labeled from the simulation neglecting the ion dynamics. Two dashed vertical lines indicate two time moments: $\omega t = 34.31$ and $\omega t = 36.62$.

0.25 V/m as demonstrated in Figure 7. The strength of this component will be larger when the higher voltage is applied to the antenna. If this value was the electric field amplitude of the transmitted whistler wave, it would be much stronger than the electric field amplitude of the natural whistler waves in the inner magnetosphere, which is typically in the order of mV/m [e.g., *Helliwell*, 1965; *Meredith et al.*, 2001]. Note that once the whistler waves are excited in the plasma around the antenna, the wave energy is confined in a small angle with respect to geomagnetic field lines and is not damped very much along its field-aligned guided propagation path. Thus it may be feasible to use the whistler wave transmitted from high-voltage antennas in the magnetosphere for controlled precipitation of relativistic electrons in the radiation belts. We should, however, keep in mind that a definite conclusion cannot be derived from the present simulation which is quasi-static in nature. We will further examine this issue with the simulations that include the magnetic fields and thus can deal with the wave transmission directly.

4. Effects of Ion Dynamics on Antenna–Plasma Interaction

[34] The simulation results shown above reproduce the theoretical predictions by *Song et al.* [2007], indicating that the simulation model is reliable. Such a simulation without the ion dynamics is illustrative and is valid if the frequency of the antenna current is much higher than the ion characteristic frequencies. As argued in the Introduction, in the inner magnetosphere the VLF wave frequencies may not be much higher than the ion characteristic frequencies so that ion dynamics should be included. In this section we examine how the ion dynamics affects the antenna–plasma interaction. In the present simulation, both the ions and electrons move in response to the time-dependent electric field. We use the same simulation parameters described at the beginning of section 3. The oscillating frequency of the antenna current utilized, 30 kHz, is only about 6 times the ion plasma frequency (~4.8 kHz for the given plasma density of 500 cm^{-3}). The effects of the ion dynamics thus should be clearly observable in the simulation.

[35] We first examine how the antenna charging is affected by the ion dynamics. Figure 8 shows, in the same format as that of Figure 2, the results from the simulation with the ion dynamics included. The antenna charging is still completed within about one-fourth of an oscillating period as can be seen from the time variation of the antenna charge density. A readily noticeable feature is that, in contrast to the case without the ion dynamics, the peak value of the antenna charge density is slightly positive in the present simulation. Consequently, the antenna electric field from the simulation with mobile ions has a short excursion of small positive values in each oscillation cycle. The positive excursion of the antenna charge density and electric field is caused by the ion current collected by the antenna from the plasma as will be discussed later.

[36] Same as in the case without the ion dynamics, it is demonstrated by Figure 8 that the antenna potential is also nearly $-90°$ out of phase with the antenna current. Averaged over 6 oscillation periods, the potential–current phase difference is about $-88.79°$ and the peak-to-peak antenna

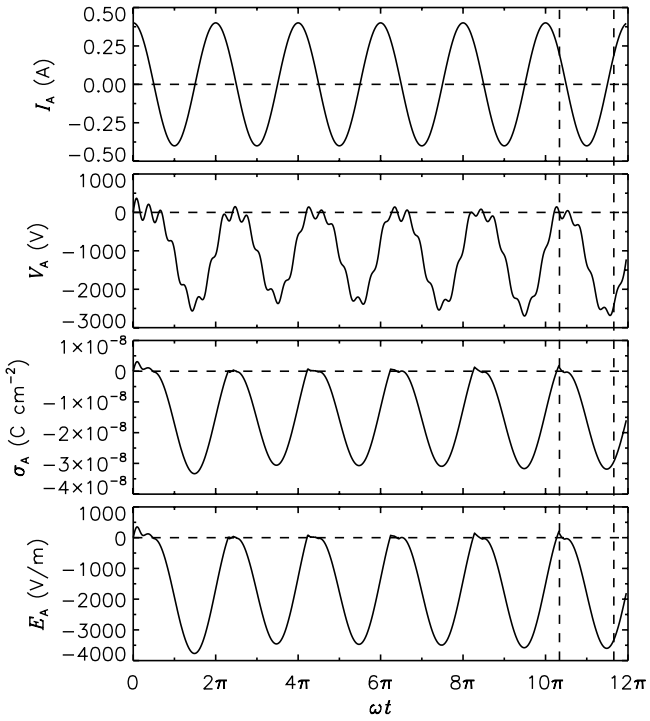

Figure 8. The same format as that of Figure 2 but for the simulation with the ion dynamics included. Two dashed vertical lines indicate two time moments: $\omega t = 32.48$ and $\omega t = 36.62$.

potential difference is about 2741.48 V. The antenna reactance is then calculated to be about 3426.1 Ω, close to the reactance (3486.2 Ω) obtained from the simulation without the ion dynamics included. Including the ion dynamics in the simulation, therefore, does not significantly affect the antenna reactance for the simplified 1D and quasi-static situation.

[37] In Figure 9 we display electron (solid line) and ion (dotted line) current collected by the antenna because of the electrons and ions impinged on the antenna surface. Also plotted, as stars, is the total (electron plus ion) current

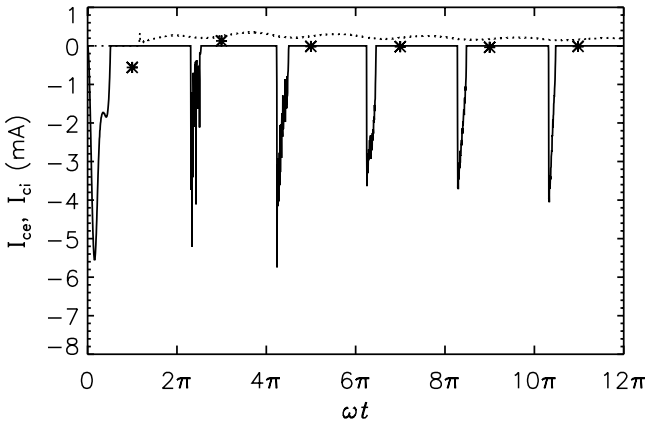

Figure 9. Electron (solid line) and ion (dashed line) current collected by the antenna as a function of time. Stars represent the total (electron plus ion) current averaged over each oscillation period.

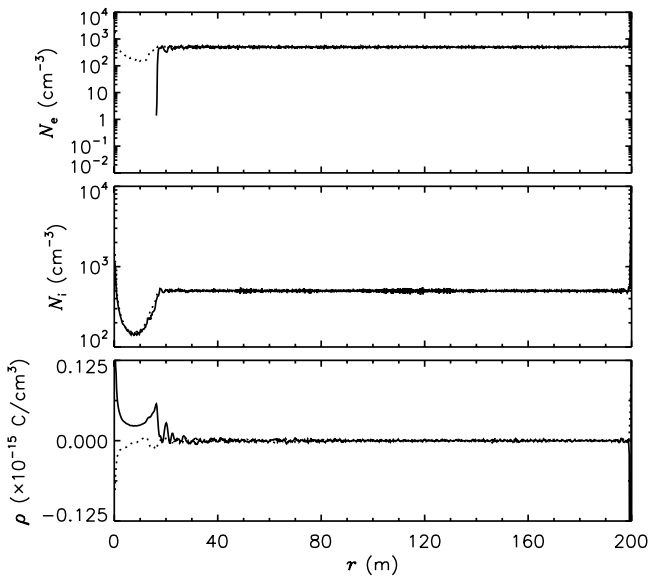

Figure 10. Electron density (first panel), ion density (second panel), and charge density (third panel) distribution at $\omega t = 32.48$ (dotted line) and $\omega t = 36.62$ (solid line), corresponding to the time moments indicated by two dashed vertical lines in Figure 8.

averaged over each oscillation period. First of all we note that the electron current (or the electron impinging to the antenna) is impulsive with the oscillation period of the antenna current. The first pulse occurs in the first one-fourth period, which causes the negative charging of the antenna. The negative charging results in a negative electric field that repels the electrons away but attracts the ions toward the antenna. After the first half oscillation cycle of the antenna current, the ion current starts with a small peak value. The ion current is continuous since the collection of ions by the antenna is continuous. The ion collection does not stop even when the total charge density (sum of ions and electrons attracted from the plasma and charge from the antenna current) on the antenna becomes positive. The reason is that the ions response to the electric field (and its change) slowly as a result of their large inertial compared to that of the electrons. Only when the positive charge density (so the positive electric field) lasts long enough, will the ion current disappear. Once the antenna charge density becomes positive, however, a large number of electrons rapidly flow to and reside on the antenna surface in response to the positive electric field, decreasing the antenna charge density to negative in a short time, less than one-fourth of a period. Afterward the ion current collection increases again before it completely disappears. It is also found that both the electron and ion currents collected by the antenna, are in the order of 1 mA, which is very weak compared to the peak antenna current of 0.4 A. Finally, it is shown by the stars in Figure 9 that after about 1 oscillation period, the ion current basically balances the electron current averaged over each oscillation period. Thus, after the antenna charging is finished, there is no significant net conduction current to the antenna from the sheath, which is consistent with the IMAGE RPI experiment discussed by *Song et al.* [2007].

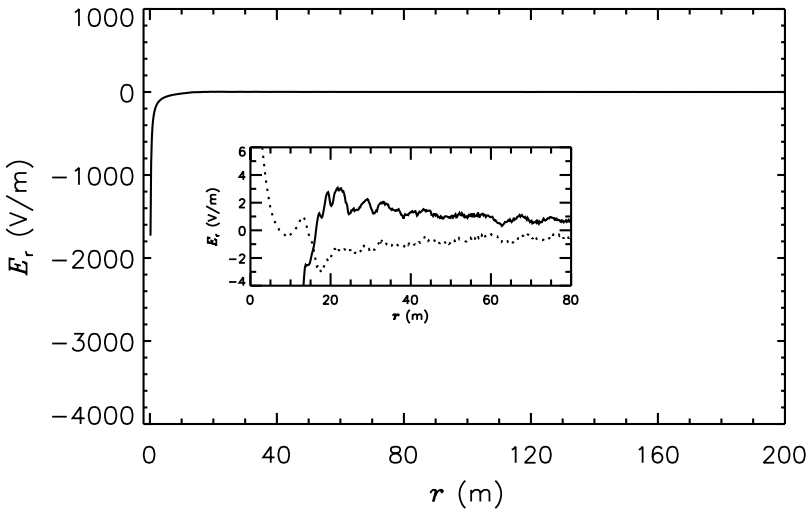

Figure 11. The electric field distribution at $\omega t = 31.30$ from the simulation with the mobile ions. The inserted figure displays fine structures of the electric field around the sheath–plasma boundary at $\omega t = 31.30$ (solid line) and $\omega t = 32.48$ (dotted line).

[38] Next we examine how the plasma sheath structures are affected by the ion dynamics. It is found by scrutinizing the individual density snapshots that the electron density distribution consists of similar structures to those in the simulation without the ion dynamics, when the antenna charge density (and also the antenna electric field) is negative. There is a region of the deeply depleted electron density (essentially zero) with a sharp density gradient at the outer boundary. The boundary moves in and out when the negative charge density on the antenna decreases and increases in magnitude. However, the electron density distribution is distorted substantially from above picture during the positive excursion of the antenna charge density. As an example, we show in Figure 10, from the first to the last panels, the electron density, ion density and charge density distribution at $\omega t = 32.48$ (dotted line) and $\omega t = 36.62$ (solid line), corresponding to the time moments indicated by the two dashed lines in Figure 8, respectively. The deeply depleted region in the electron density distribution is observed at $\omega t = 36.62$ similar to that shown in Figure 4. Nevertheless, at $\omega t = 32.48$ when the antenna charge density becomes positive, the electron density distribution is quite different: the deeply depleted region is now filled in with the electrons although the density inside the region is still lower than the background. Filling the depleted region is simply due to the inward attraction of the electrons by the positive electric field. The U-shaped structure is caused by the rapid attraction of the electrons in the vicinity of the antenna while slower supply of the electrons from background plasma region where the electric field is much weaker. The charge density at $\omega t = 32.48$ in the U-shaped region is negative because of the extra electrons. In other words, there is an electron plasma sheath at this moment. This is different from the situation without the ion dynamics where there always exists an ion plasma sheath.

[39] The ion density distribution is also U-shaped: decreased in the center of the region while enhanced (above its background value) in the immediate proximity of the antenna. The enhanced ion density near the antenna is caused by the negative electric field which attracts the ions toward the antenna. The valley of the ion density is a result of attraction of the ions to the vicinity of the antenna and the slow supply of the ions to the valley region from the plasma. Such an ion density structure is quite stable as demonstrated by comparing the ion density distributions at $\omega t = 32.48$ (dotted line) and $\omega t = 36.62$ (solid line) shown in Figure 10. The persistence of the U-shaped structure during the positive excursion of the electric field is resulted from the finite response time of the ions to the electric field and the short period of the positive electric field.

[40] As in the case without the ion dynamics, the plasma sheath tends to shield the electric field from penetrating into the plasma. The shielding, however, is even less perfect in the present simulation. A significant electric field, which has a component oscillating at the frequency of the antenna current, extends farther into the plasma. Figure 11 demonstrates the electric field distributions at $\omega t = 31.30$. The fine structures of the electric field around the plasma sheath boundary is also shown for the time of $\omega t = 31.30$ (solid line) and $\omega t = 32.48$ (dotted line) by the inserted panel. It is seen again the strength of the electric field quickly decreases away from the antenna and becomes weak beyond the plasma sheath. As shown by the inserted panel, the amplitude of the electric field is around 1 V/m, which is significant. Note that at $\omega t = 32.48$ the electric field in the sheath is positive because of the positive antenna charge density at that time.

5. Summary and Discussions

[41] We have applied a PIC simulation code to investigate the antenna–plasma interaction in space plasma. We performed the simulations for cases without and with ion dynamics included. By assuming that ions do not move, the simulation performed with our 1D code basically reproduces the theoretical predications by *Song et al.* [2007], namely, antenna charging, ion plasma formation, and the oscillation of the sheath radius. The simulation also reveals the details of the antenna charging process and the

fine structures of the plasma sheath, which are not tractable by the analytical methods. It is seen from the simulation that the antenna charging and the plasma sheath formation is a transit dynamic process that is completed in about one-fourth of an oscillation cycle. The sheath radius oscillates with the frequency of the antenna driving current and has a finite minimum value. Furthermore, the electric field oscillations at the plasma frequency in the plasma, which are not expected in the analytical model, are clearly demonstrated by the simulation. The simulation including the ion dynamics reveals a number of new features of the antenna–plasma interaction. These features include a brief excursion of the positive antenna charge density and electric field, the impulsive electron and continuous ion currents collected by the antenna, electron plasma sheath during the excursion of the positive antenna charge density, and stable U-shaped ion density structure in the plasma sheath region. The antenna reactance evaluated from the simulations with and without the ion dynamics are nearly the same. The simulations improve the reactance value from the theoretical estimate given by *Song et al.* [2007] by about 10%. Such improvement demonstrates the advantage of the PIC simulation models that can include the plasma sheath effects self-consistently in studying the antenna–plasma interaction.

[42] In the simulations, the plasma sheath is formed as a result of the negative antenna charging. This is similar to the formation of a Debye sheath around an electrode (or a probe) in the plasma. However, the sheath size (or radius in cylindrical geometry) is controlled primarily by the strong electric field excited by the antenna charge instead of the Debye length (or plasma temperature) because the transmission antenna is actively driven. That is, the sheath formation is caused by the kinetic force of the applied electric field rather than the difference between the thermal motions of the electrons and ions. As shown by Figure 5, although the plasma is assumed cold, the simulated sheath size is of a spatial scale comparable to the Debye length of a 1-keV warm plasma with the same density as that used in the simulations (500 cm^{-3}). In addition, different from the case of the Debye sheath, the potential and electric field are not zero at the plasma sheath boundary, which itself oscillates with the antenna current frequency. Actually there is an electric field component with a significant amplitude ($\sim$0.3 V/m) oscillating at the frequency of the antenna current because of the partial penetrating of the electric field into the plasma. If this is the amplitude of the transmitted whistler wave, it is strong compared to the amplitude (typically in the order of mV/m) of the natural whistler waves in the magnetosphere [*Helliwell*, 1965; *Meredith et al.*, 2001], implying the applicability of the high-voltage antennas in whistler wave transmission. Nevertheless, simulations that include the magnetic fields are necessary for a definite conclusion on this issue.

[43] The simulations provide significantly improved understanding of the antenna–plasma interaction in the context of high-voltage antennas in the inner magnetosphere, although they were performed on the basis of several assumptions, namely, cold plasma, negligible end effects at the antenna tips, weak effects of the magnetic field, and thus the 1D approximation. Including those effects neglected in the present simulations will allow more accurate evaluation of the impedance properties of the antennas and comprehensive understanding of the antenna transmission characteristics in the presence of the plasma sheath.

[44] **Acknowledgments.** This work was supported by AFRL under contracts F19628-02-C-0092 and FA8718-05-C-0070. J. Tu thanks X. Huang for many thoughtful discussions. The authors greatly appreciate the suggestive comments from the reviewers.

[45] Amitana Bhattacharjee thanks Paul J. Kellogg and another reviewer for their assistance in evaluating this paper.

References

Baker, D. J., H. Weil, and L. S. Bearce (1973), Impedance and large signal excitation of satellite-borne antennas in the ionosphere, *IEEE Trans. Antennas Propag.*, *21*, 672–679.

Balmain, K. G. (1964), The impedance of a short dipole antenna in a magnetoplasma, *IEEE Trans. Antennas Propag.*, *12*, 605–617.

Birdsall, C. K., and A. B. Langdon (1983), *Plasma Physics via Computer Simulation*, 479 pp., McGraw-Hill Book Company, New York.

Dum, C. T. (1984), Simulation models for space plasmas and boundary conditions as a key to their design and analysis, in *Computer Simulation of Space Plasmas*, edited by H. Matsumoto and T. Sato, pp. 303–375, Terra Scientific Publishing, New York.

Helliwell, R. A. (1965), *Whistlers and Related Ionospheric Phenomena*, 368 pp., Stanford Univ. Press, Stanford, Calif.

Hockney, R. W., and J. W. Eastwood (1988), *Computer Simulation Using Particles*, 540 pp., Taylor and Francis, New York.

Inan, U. S., T. F. Bell, J. Bortnik, and J. M. Albert (2003), Controlled precipitation of radiation belt electrons, *J. Geophys. Res.*, *108*(A5), 1186, doi:10.1029/2002JA009580.

Kuehl, H. H. (1966), Resistance of a short antenna in a warm plasma, *Radio Sci.*, *1*, 971–976.

Laframboise, J. G., and L. J. Sonmor (1993), Current collection by probes and electrodes in space magnetoplasmas: A review, *J. Geophys. Res.*, *98*, 337–357.

Meredith, N. P., R. B. Horne, and R. R. Anderson (2001), Substorm dependence of chorus amplitudes: Implications for the acceleration of electrons to relativistic energies, *J. Geophys. Res.*, *106*, 13,165–13,178.

Mlodnosky, R. F., and O. K. Garriott (1963), The v.l.f. admittance of a dipole in the lower ionosphere, in *Proc. Int. Conf. Ionosphere*, pp. 484–491, Inst. Phys. and Phys. Soc., Dorking, U. K.

Morin, G. A., and K. G. Balmain (1993), Plasma sheath and presheath waves: Theory and experiment, *Radio Sci.*, *28*, 151–167.

Nakatani, D. T., and H. H. Kuehl (1976), Input impedance of a short dipole antenna in a warm anisotropic plasma: 1. Kinetic theory, *Radio Sci.*, *11*, 433–444.

Nikitin, P., and C. Swenson (2001), Impedance of a short dipole antenna in a cold plasma, *IEEE Trans. Antennas Propag.*, *49*, 1377–1381.

Oliver, B. M., R. M. Clements, and P. R. Smy (1973), Experimental investigation of the low-frequency capacitive response of a plasma sheath, *J. Appl. Phys.*, *44*, 4511–4517.

Reinisch, B. W., et al. (2000), The radio plasma imager investigation on the IMAGE spacecraft, *Space Sci. Rev.*, *91*, 319–359.

Riemann, K.-U. (1991), The Bohm criterion and sheath formation, *J. Phys. D: Appl. Phys.*, *24*, 493–518.

Shkarofsky, I. P. (1972), Nonlinear sheath admittance, currents, and charges associated with high peak voltage drive on a VLF/ELF dipole antenna moving in the ionosphere, *Radio Sci.*, *7*, 503–523.

Song, P., B. W. Reinisch, V. Paznukhov, G. Sales, D. Cooke, J.-N. Tu, X. Huang, K. Bibl, and I. Galkin (2007), High voltage antenna–plasma interaction in whistler wave transmission: Plasma sheath effects, *J. Geophys. Res.*, *112*(A3), A03205, doi:10.1029/2006JA011683.

Tsutsui, M., I. Nagano, H. Kojima, K. Hashimoto, H. Matsumoto, S. Yagitani, and T. Okada (1997), Measurements and analysis of antenna impedance aboard the Geotail spacecraft, *Radio Sci.*, *32*, 1101–1126.

Ward, J., C. Swenson, and C. Furse (2005), The impedance of a short dipole antenna in a magnetized plasma via finite difference time domain model, *IEEE Trans. Antennas Propag.*, *53*, 2711–2718.

Zhao, H., R. Schmidt, C. P. Escoubet, K. Torkar, and W. Riedler (1996), Self-consistent determination of the electrostatic potential barrier due to the photoelectron sheath near a spacecraft, *J. Geophys. Res.*, *101*, 15,653–15,659.

B. W. Reinisch, P. Song, and J. Tu, Center for Atmospheric Research, University of Massachusetts–Lowell, 600 Suffolk Street, Lowell, MA 01854-3629, USA. (jiannan_tu@uml.edu)